An AC Impedance Spectroscopic Study of Li_xCoO_2 at Different Temperatures

F. Nobili, R. Tossici, and R. Marassi*

Dipartimento di Scienze Chimiche, Università di Camerino, 62032 Camerino, Italy

F. Croce* and B. Scrosati

Dipartimento di Chimica, Università di Roma "La Sapienza", 00185, Roma, Italy

Received: September 19, 2001; In Final Form: December 18, 2001

An AC impedance spectroscopic study of the Li_xCoO_2 electrode in the temperature range of 0−30 °C is presented. The results are interpreted on the basis of an equivalent circuit that includes elements related to the electronic and ionic transport in addition to the charge transfer process. The evolution of the impedance spectra with the temperature shows that a thermally activated insulator to metal transition occurs at the beginning of the deintercalation process. At intermediate intercalation degrees, the effects of the finite electronic conductivity of the material and of the charge transfer process clearly appear as separate features in the spectra at low temperature.

Introduction

For over 10 years, $LiCoO_2$ has been used as positive electrode material in commercial lithium-ion batteries.[1,2] Despite the large number of experimental and theoretical papers[3−14] that appear regularly in the literature on $LiCoO_2$ and, in general, on the other members of the family $Li_xNi_{1-y}Co_yO_2$, a debate is still open on the electronic conductivity, electronic structure, phase transitions, their effect, and the electrochemical performances. The literature data[6,7,15−19] leave no doubts about the existence of a drastic change of the electronic conductivity occurring at the early stage of lithium deintercalation and caused by an insulator to metal transition. In the case of $LiCoO_2$, the transition has been proposed to be responsible for the existence of a two phase region between the Li concentrations of $x = 0.93$ and 0.75.[4] The drastic change in resistance caused by the insulator to metal transition must necessarily be reflected in the impedance dispersion. However, the high impedance values[20−26] at the beginning of the deintercalation are either discarded on the assumption that the electrodes are blocking[25] or attributed to the charge-transfer resistance. Hence, the effects of the insulator to metal transition are underestimated. This may have been favored also by the fact that the fully intercalated phase is believed to be difficult to restore during discharge after the first deintercalation.[19]

In recent papers,[27−29] the AC impedance of compounds of the series $LiCo_yNi_{1-y}O_2$ have been studied with special attention to the ionic and electronic conductivity. It was found that the large variation in the conductivity in the x range between 1 and 0.9 is clearly reflected by the AC spectra also in cycled electrodes. The inclusion in the equivalent circuit of an element related to the electronic conductivity results in a more realistic picture of the physical phenomena occurring during the deintercalation process.

The present paper presents an electrochemical impedance study (EIS) of $LiCoO_2$ electrodes at various temperatures. Particular attention has been paid to the study of the temperature dependence of spectral features in order to discriminate between thermally and not thermally activated physical properties.

Experimental Section

The electrodes were prepared by spraying a dispersion of $LiCoO_2$ (Merck, battery grade), poly(vinyl chloride) (PVC; high molecular weight, Fluka), and acetylene black carbon (90:5:5 w/o) on a 10 μm thick high purity aluminum foil. The electrodes were dried at 120 °C under vacuum for at least 24 h before being inserted into the electrochemical cell. The loading of the electrodes was of the order of 1.5 mg/cm^2 of active mass.

The measurements have been performed using T-shaped polypropylene Swagelock type cells equipped with stainless steel (SS304) current collectors. Disks of high-purity lithium foil by Foote Mineral Co. were used as counter and reference electrodes. The electrolyte was a 1M solution of $LiClO_4$ in ethylene carbonate−dimethyl carbonate (EC-DMC 1:1, Merck battery grade). A polypropylene film (Celgard 2501, Celanese Co.) was used as separator. The cells, assembled into an argon filled drybox with moisture and oxygen content below 2 ppm, were cycled two times between 3.5 and 4.2 V at very slow rate (current rate 100 μA) to achieve a steady-state behavior. After this step, the cells were opened in the box to eliminate any possible gas developed during SEI (solid electrolyte interface) formation on the electrodes. The resealed cells were operated outside the box using a silicon oil bath to regulate the temperature.

All of the measurements were performed using a CH650 electrochemical station (CH Instruments, Cordova TN) driven by a PC. The impedance spectra (1 mHz to 100 kHz, 10 mV perturbation) were recorded at five different temperatures in the range of 0−30 °C. The sequence of operation consisted of a loop comprising a potentiostatic step (generally 10 mV) at the higher temperature followed by an equilibration time of at least 5 h and by recording of the AC spectra taken at each temperature (allowing a sufficient equilibration time after each temperature variation).

* To whom correspondence should be addressed. E-mail: marassi@camserv.unicam.it. E-mail: fausto.croce@uniroma1.it.

10.1021/jp013569a CCC: $22.00
Published on Web 03/22/2002

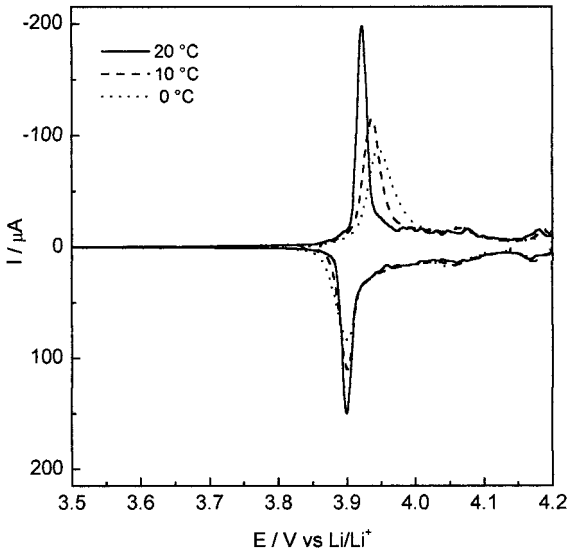

Figure 1. Cyclic voltammograms of an $LiCoO_2$ electrode taken at different temperatures. Scan rate 10 μV s^{-1}.

Results and Discussion

Figure 1 shows some sample slow scan rate cyclic voltammograms obtained at different temperatures. The shape of the curves closely resemble those reported in the literature by several authors.[20,26] The curve traced at 20 °C is relative to a freshly prepared electrode, whereas the others reflect the steady-state behavior at the different temperatures. The decrease of the temperature causes a shift in the positive direction of the peak potential of the deintercalation wave. The shift is accompanied by an increase in the half peak width indicating a decreased reversibility. On the contrary, the temperature does not seem to affect much the intercalation process.

The integrated curves have been used to calculate the quasithermodynamic *x* versus *E* curves in order to assign a value of the intercalation degree (*x*) to each potential. The integrated curves reveal a loss of capacity of about 7% between the first and second polarization due to partial solvent decomposition[6] and SEI formation (see below). No appreciable capacity loss has been found after the first cycle. Because of the uncertainty introduced by the capacity loss during the first potential polarization, the calculated *x* probably contains some bias and should be taken with some care.

Figure 2a,b shows a sequence of characteristic Nyquist plots obtained at constant temperature and at potentials far from the deintercalation peak. The trend of the dispersions is typical for compounds of the $LiMO_2$ family (with M = Co, Ni, or a mix of the two).[27−29] The dispersions are characterized by a great semicircular arc in the low-frequency region that is strongly potential dependent and shows an increasing tendency to close on the real axis as the potential becomes more positive. This is accompanied by a decrease of at least 3 orders of magnitude of the overall impedance. At any of the potentials, a not well defined semicircle is present at the high frequency limit. As the potential approaches the foot of the deintercalation peak shown in Figure 1, the low frequency semicircle becomes progressively smaller, whereas a second semicircle starts to become evident in the middle frequency range together with the characteristic signature of thin-layer ionic diffusion (Figure 2b).

Figures 3a,b and 4a,b show the Nyquist plots obtained at various temperatures and different potentials. Figure 3 refers to potential values for which the computed *x* value is above

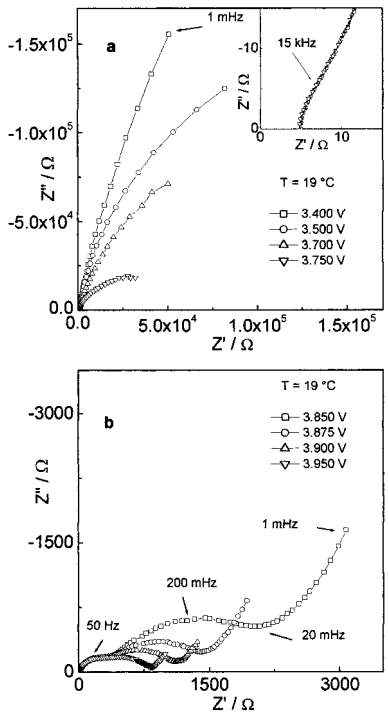

Figure 2. Series of Nyquist plots obtained at 19 °C at different potentials: (a) potential range from 3.4 to 3.75 V vs Li; (b) potential range from 3.85 to 3.95 V vs Li/Li^+.

0.95 and hence to a region where the compound is supposed to be an insulator. In general, the absolute impedance increases markedly with decreasing temperature. At the higher potential (Figure 3a, $x \cong 0.99$), the tendency of the low frequency semicircle that dominates the dispersion to close on the real axis becomes progressively more evident as the temperature increases. At 3.85 V ($x \cong 0.96$, Figure 3b) where, following the literature data a two phase region starts to appear,[6] apart from the temperature effect, the dispersions show the main features previously described. When the potential is further increased (Figure 4a,b), the presence of two distinct semicircles in the middle and low frequency region becomes more and more evident as the temperature decreases. For sake of clarity, each dispersion is shifted by 500 ohm on the *y* scale. The ill-defined depressed semicircle present at the 24 °C in both graphs splits progressively into two distinct semicircles that become fully developed at the lowest temperature.

When the present results and those previously obtained at room temperature on compounds of the series $Li_xNi_{1-y}Co_yO_2$,[27−29] including the extreme Li_xCoO_2 and Li_xNiO_2, with those of other workers are compared,[20−26] it turns out that the main difference is relative to the presence of two semicircles in the middle and low frequency region. The present results further support our previous results as the temperature clearly enhances the separation of two different physical phenomena by affecting in a different way the relative time constants. In the previous papers,[27−29] the EIS spectra were interpreted in terms of the following physical phenomena in order of decreasing frequency: (i) a high-frequency dispersion (>1 kHz) because of presence of a passivating layer, (ii) an intermediate frequency dispersion (between 10 Hz and 1 kHz) because of charge transfer, (iii) a low-frequency semicircle associated with the electronic properties of the material, and finally, (iv) the very low-frequency spike of the ionic diffusion. The hypothesis to assign the low-frequency semicircle (iii) to the electronic resistance of the material and the middle one (ii) to the charge-

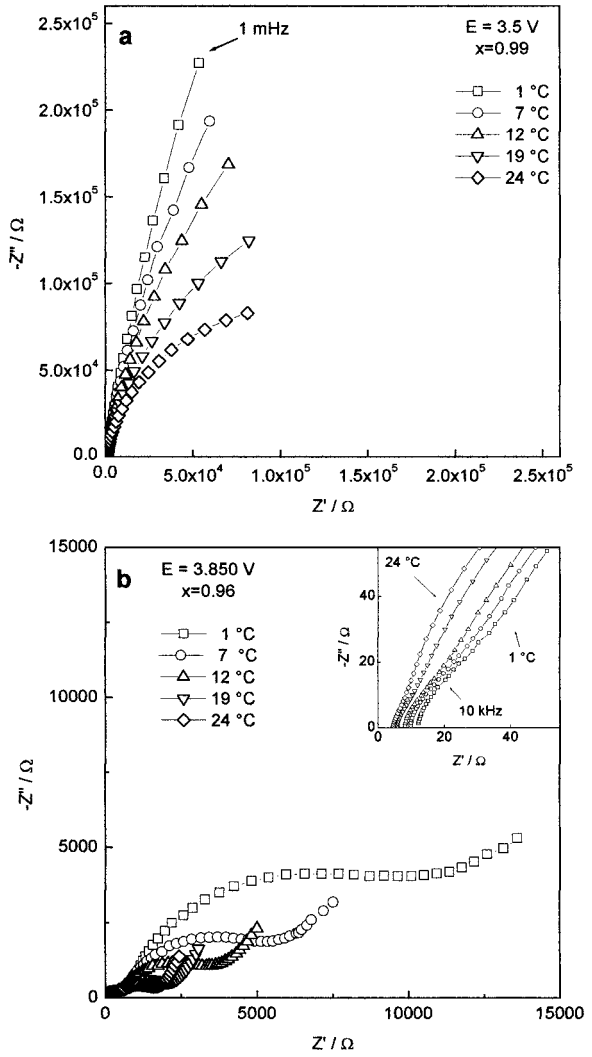

Figure 3. Series of Nyquist plots obtained at different temperatures: (a) $E = 3.5$ V vs Li/Li^+ ($x \cong 0.99$); (b) $E = 3.85$ V vs Li/Li^+ ($x \cong 0.96$).

transfer process was based on the following two reasons: (i) the drop of the resistance associated with the low-frequency semicircle occurs over the narrow x range that corresponds to the insulator to metal transition and (ii) the growth of the additional semicircle in the middle frequency range becomes appreciable in correspondence of potential values at which the intercalation process starts to take place at an appreciable rate. In addition, it should be observed that, in the case of $Li_xNi_{0.25}Co_{0.75}O_2$ at room temperature, the potential variation[27] of the resistance associated with the low-frequency semicircle was independent of the direction of polarization, i.e., spectra taken during a positive (deintercalation) or negative (intercalation) run. This somewhat contrasts with the common perception[6,19] that the fully intercalated phase is difficult to restore during discharge because of kinetic problems caused by the difficulty to intercalate lithium when the nature of the compounds become close to electronically insulating materials.

In previous work, the data have been fitted with Boukamp's equivalent circuit program,[30] using the equivalent circuit of Figure 5, similar to the one used by Levi and co-workers.[20] The three RC parallel (in the simulation, Q, the costant phase element defined in ref 29, has been used instead of C) elements in series describe the surface layer, the charge transfer, and the electronic resistance, respectively. The circuit includes, in addition, the electrolyte resistance, the Warburg diffusive impedance, and a capacitor representing the intercalation capacity.

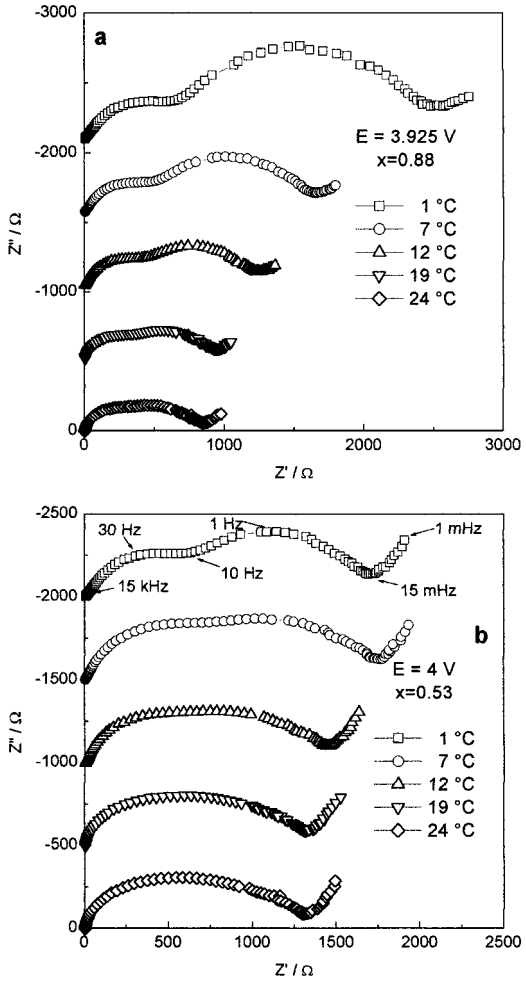

Figure 4. Series of Nyquist plots obtained at different temperatures: (a) $E = 3.95$ V vs Li/Li^+ ($x \cong 0.88$); (b) $E = 4$ V vs Li/Li^+ ($x \cong 0.0.53$). Each curve is displaced of 500 Ω on the y axis.

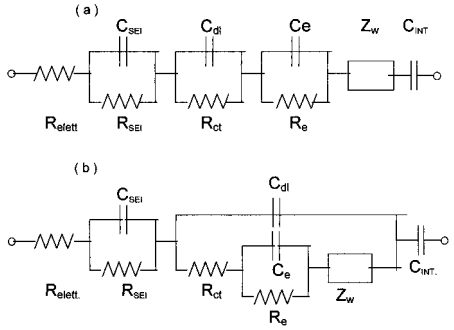

Figure 5. Equivalent circuits used to simulate the data. (a) Levi and co-workers, ref 20; (b) Bruce and Saidi, ref 30.

One possible alternative to the equivalent circuit in Figure 5a is the one shown in Figure 5b. The circuit is a modification of the one proposed by Bruce and Saidi[31] for the intercalation of Li^+ in TiS_2 electrodes using the adatom model. The electrolyte resistance and the intercalation capacity are in series with a parallel element that includes a Randles type[32] circuit to which a parallel RC element has been added. In the original formulation of Bruce and Saidi,[3] the latter parallel was composed by a resistance (R_{latt}, resistance to lattice incorporation) and a capacity (C_s, adatom-pseudo capacity) in series with an element (Z_{cpa}) to take into account the rough nature of the electrode.

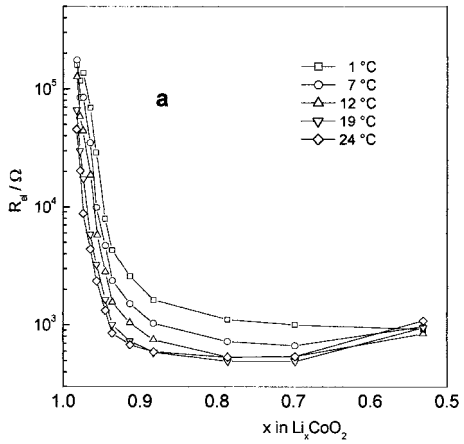

Figure 6. Plots of (a) electronic resistance (R_e) vs intercalation degree (x) at different temperatures.

Both circuits give rise to three semicircles in the dispersion. From the pure electrical point of view, the two circuits are equivalent, and the experimental data can be satisfactorily fitted using both of them with only slight differences in the goodness of the fit (average values of χ^2 are of the order of 10^{-4} and 10^{-5}, for circuits a and b, respectively, lower values have been found at low potential where the large semicircle due to the electronic conductivity dominates the spectra). However, the adatom model, as adapted by Bruce and Saidi[31] to describe intercalation electrodes, seems to be closer to the physics of the process than a mere series of elements able to simulate the data. In addition, it has important consequences as far as, for instance, the charge transfer resistance is concerned. Basically, in the adatom model, the intercalation−deintercalation process is described in terms of partially desolvated lithium ions that are adsorbed on the electrode surface. The process is accompanied by the insertion of an electron into the conduction band of the host followed by diffusion of Li^+ to the intercalation site where it becomes fully incorporated into the lattice. The rate determining step is the incorporation of Li ions into the lattice, and as a consequence, it follows that the charge-transfer resistance is potential independent. The model was developed for the case of intercalation in TiS_2 which is a good electronic conductor. In the present case, metallic conductivity is reached only for $x > 0.95$, and hence, during the early stages of deintercalation, the electron flow is limited by the low conductivity of the material, and the incorporation of lithium ions into the lattice are practically inhibited. In other words, lattice incorporation and electron conduction appear to be the opposite faces of the same phenomena. Along this line, the parameter R_{latt} in the original equivalent circuit of Bruce and Saidi has been substituted by R_e, electronic resistance. The associated capacity Q_e includes the constant phase angle element that takes into account the rough nature of the electrode.

Figures 6−8 show the variation of the different parameters with x at the different temperatures, as deduced from the simulation using the equivalent circuit in Figure 5b. As may be seen, the parameter associated with the electronic resistance (Figure 6) falls by about 3 orders of magnitude over a narrow x range from $x \cong 1$ to 0.9. This is consistent with the trend already found for the compounds of the family[27−29] $Li_xNi_{1-y}Co_yO_2$. The corresponding apparent conductivity, computed as reciprocal of R_e, resembles the one measured in situ using microarray electrodes.[18,19] The resistances at any x increase, and consequently, the conductivity decreases, with decreasing temperature. The capacities in parallel to R_e, C_e (Figure 8a), are very high (in the range of hundred of microfarad) and follow

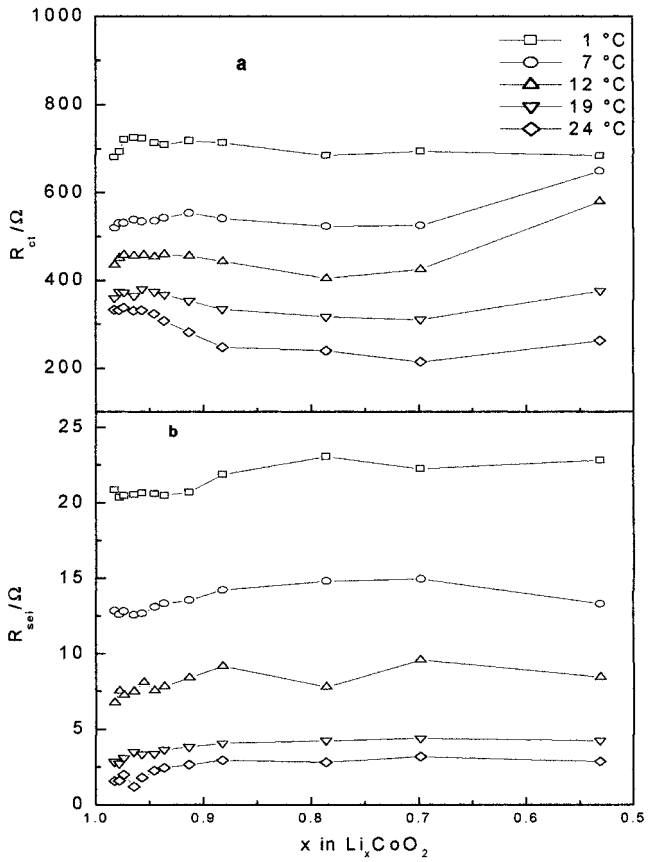

Figure 7. Plots of (a) charge-transfer resistance (R_{ct}) and (b) surface layer resistance (SEI) vs intercalation degree (x) at different temperatures.

the same trend of the resistances. The high values of C_e explain the appearance of the semicircular dispersion related to electrical conductivity in the low-frequency region of the impedance spectra. A possible physical explanation for the presence of this capacity, that following the proposed model includes a contribution because of the rough nature of the electrode, is the formation of capacitors because of electron accumulation at the nanosize crystallite domains of the material.[33] If the model is correct and the low frequency semicircle is indeed correlated with the electronic conductivity of the material, the temperature dependence should reflect the activated nature of the nonmetal to metal transition. This is indeed the case, as shown in Figure 9a,b that show the Arrhenius plots of the apparent electronic conductivity and the plots of the activation energies as a function of x, respectively. As may be seen, at least over the limited temperature range explored, the plots are linear with slope decreasing rapidly with decreasing x. The activation energy drops from about 0.4 eV for $x \cong 1$ to about 0.1 eV for $x \cong 0.9$ to become practically 0 at $x = 0.53$, when the material is a metal. The computed activation energies are of the same order of magnitude of those reported by several authors.[6,15,17]

The resistances and the capacities associated with the high-frequency semicircle (Figures 7b and 8c) are rather constant with x and increase with decreasing temperature. This indicates a rather stable passivating layer on the electrode surface. These results are consistent with those of previous workers.[21] The formation of a passivating layer on $LiCoO_2$ has been discussed by Dokko and co-workers,[26] who recently characterized single particles of $LiCoO_2$ by AC impedance and other techniques and extensively by Levi and Aurbach.[23,24] They do not exclude formation of a passivating layer because of reaction with the solvent but tend to conclude that in composite electrodes the

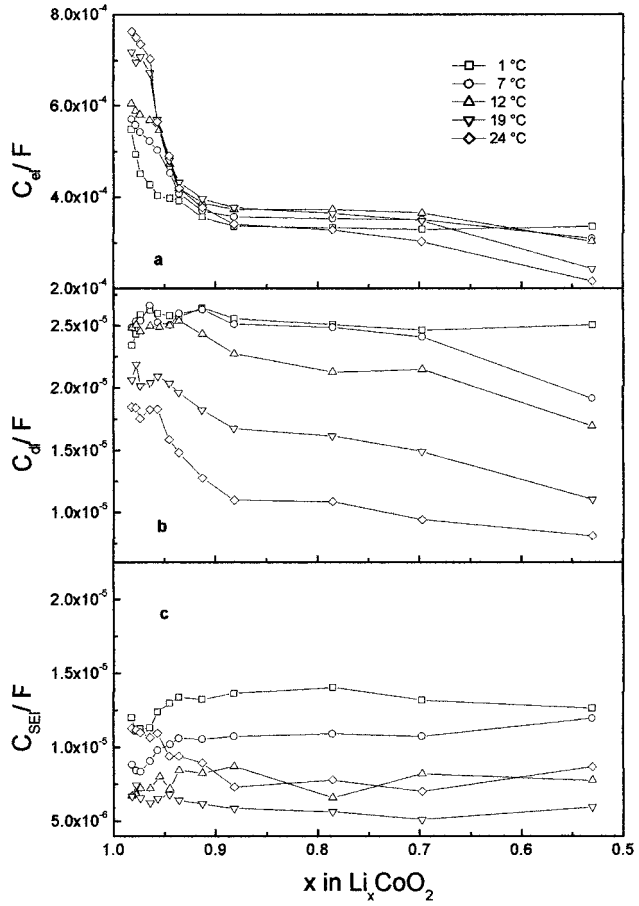

Figure 8. Plots of the capacities associated with (a) electronic resistance, (b) double layer capacity, and (c) solid electrolyte interface.

semicircle at high frequency is due to the porous structure involving carbon additive and organic binder.

With regard to the charge transfer resistance (Figure 7a) and the associated double layer capacity (Figure 8b), the relative plots show that they may be considered almost constant with *x*. This appears to be particularly true if one excludes the first points at high temperature where the medium and high-frequency semicircles are not well separated and the values derived by the fit are affected by higher uncertainties. The results, similar to those obtained for $Li_xNi_{0.75}Co_{0.25}O_2$,[28] are consistent with the model proposed by Bruce and Saidi[31] for intercalation electrodes. In conventional redox or metal deposition processes, the charge-transfer step is associated with electron tunneling between a metal electrode and an ion in solution. The rate of the electron exchange is potential dependent because the potential shifts the electronic energy levels in the metal electrode with respect to those of the incoming ion. In intercalation electrodes, where lithium exists as Li^+ in the lattice, the electrons are not transferred between the electrode and the incoming ion during the reaction but enter the host lattice to preserve the overall electroneutrality. The resulting shift in the electronic energy levels in the host does not influence the rate of charge transfer which is primarily controlled by the energetic of partial desolvation of the Li^+ ion. Figure 10 shows the plot of $1/R_{ct}$ vs $1/T$. To be noticed is the fact that, because of the usual relation $i_o = RT/nR_{ct}F$, $1/R_{ct}$ is proportional to the exchange current density. In the graph, each point is the average of the values computed at a least 17 different potential values between 3.5 and 4.1 V. The plot shows that the reaction kinetics has a single activation energy of about 0.1 eV and that it is potential independent. The data are consistent with those relative

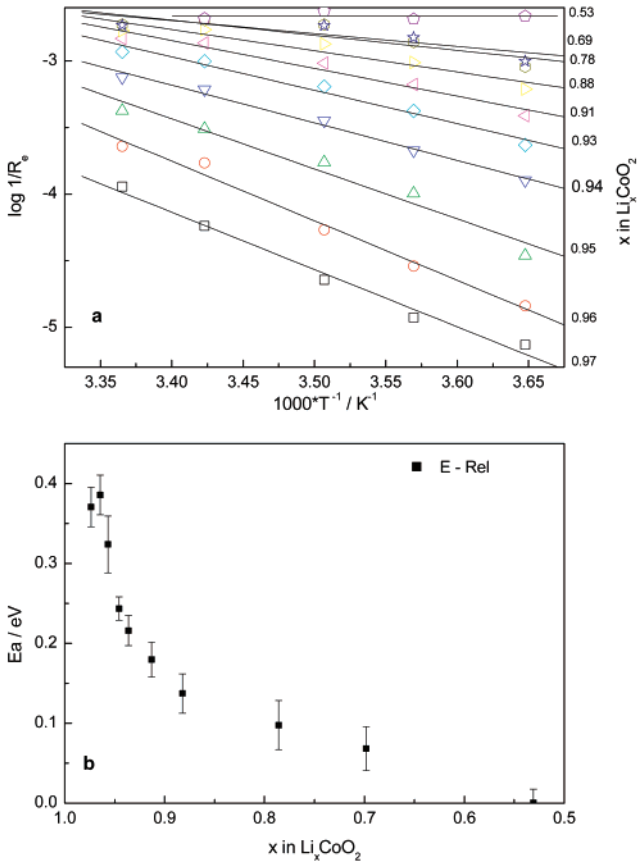

Figure 9. (a) Plots of log $(1/R_e)$ vs $1/T$ at different intercalation degrees; (b) activation energies vs *x*.

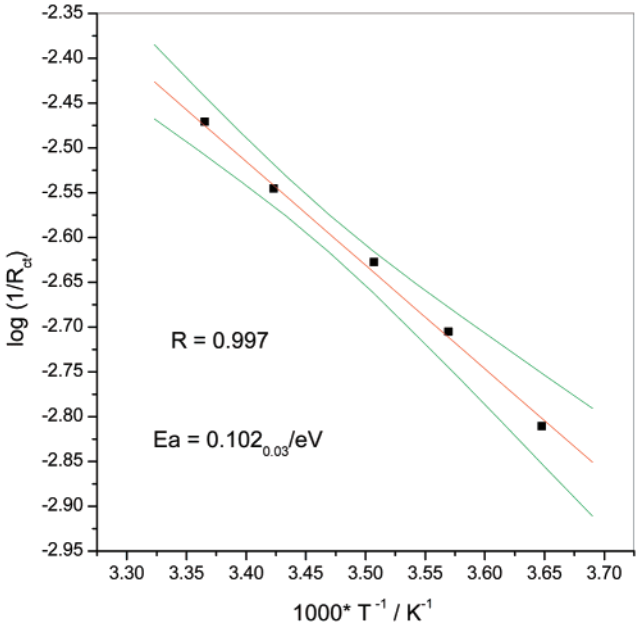

Figure 10. Plot of log $1/R_{ct}$ vs $1/T$ (see text for details). The hyperboles represent the 95% confidence limits.

to the intercalation of lithium in Na_xWO_3 as reported by Raistrick,[34,35] who suggested that the interfacial reaction is associated with ion transfer rather than with the electron transfer. The dependence of the charge-transfer resistance upon potential deserves a further comment. In discussing the relative simple dispersion obtained using a single crystal of $LiCoO_2$, Dokko et al.[26] observe that the change of R_{ct} with potential seemed to be linked to the variation of the conductivity of the material. They

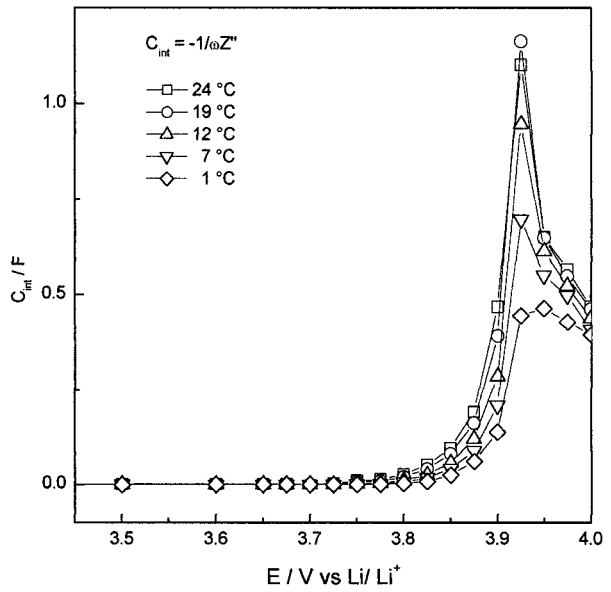

Figure 11. Plots of the intercalation capacities at the different temperatures as obtained from EIS data.

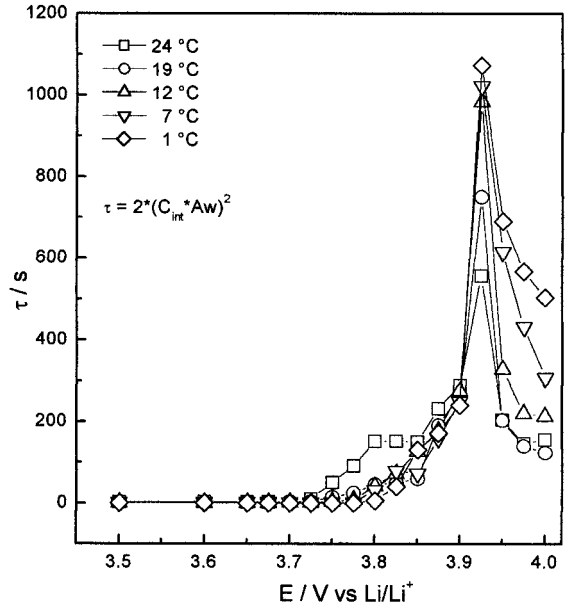

Figure 12. Characteristic diffusion time (τ) as obtained from EIS data at different temperatures.

did not further comment on this but observed that the correlation between R_{ct} and conductivity is at present not clear. The present data clearly demonstrate that electronic conductivity and ion transfer represent two different processes giving rise to different features in the AC dispersions with different time constants especially at low temperature.

Figure 11 shows the behavior of the intercalation capacity (C_L) obtained from the EIS data by modeling the experimental Nyquist plots with the equivalent circuit in Figure 5b. The data are consistent with the cyclic voltammograms in Figure 1. The differential capacity becomes lower with decreasing temperature, and at the same time, the peaks become broader as was the case for the corresponding cyclic voltammograms. The peak potentials in the cyclic voltammograms at the different temperatures correspond to those of the intercalation capacity curves.

Figure 12 shows the characteristic diffusion time τ that can be computed[20,26] from the values of the differential capacity and Warburg slope ($\tau = 2[Q_t A_W (dx/dE)^2]$)[20] as obtained by the fitting program. The characteristic diffusion time is linked to the chemical diffusion D (cm^2/s) coefficient through the diffusion length (i.e., $\tau = l^2/D$). The curve shows that τ is maximum at each temperature in the proximity of the voltammetric peak. This corresponds to a minimum in the diffusion coefficient that can be attributed to the enhancement of the attractive short-range interactions between the intercalated species.[20] As far as the diffusion coefficient is concerned, by assuming as diffusion path l the average particles size as measured by SEM ($1.5\ 10^{-4}$ cm), the estimated values of log D range from a maximum of -7 to a minimum of about -11, in line with the values quoted by other authors.[20−26] More important than the absolute value is, however, its temperature dependence. At the peak potential, the apparent chemical diffusion coefficient decreases by a factor of about 10 when the temperature is lowered from about 30 to 0 °C. This accounts for the temperature dependence of the peak currents and differential capacities.

Conclusions

EIS has been proved to be a simple and powerful technique to study not only the parameters related to the interfacial phenomena occurring at the Li_xCoO_2 electrode but also the electronic transport properties.

EIS spectra taken at different temperatures are permitted to discriminate the electronic conductivity and the charge transfer resistance. The first changes by several order of magnitude over a narrow x range ranging from $x = 1$ to about 0.95 and is thermally activated. The second is potential independent with a single activation energy being associated with ionic transfer rather than electron transfer as in a classical redox or metal deposition process.

Acknowledgment. The financial support of Ministero dell'Istruzone dell'Universitá e della Ricerca (MIUR), COFIN2000, is acknowledged.

References and Notes

(1) Mizushima, K.; Jones, P. C.; Wiseman, P. J.; Gooedenough, J. B. *Mater. Res. Bull*. **1980**, *17*, 785.
(2) Megahed, S.; Scrosati, B. *J. Power Sources* **1994**, *51*, 79.
(3) Reimers, N.; Dahn, J. R. *J. Electrochem. Soc*. **1992**, *139*, 2091.
(4) Ohzuku, T.; Ueda, A. *J. Electrochem. Soc*. **1994**, *141*, 2972.
(5) Amatucci, G. G.; Tarascon, J. M.; Uchida, I. *J. Electrochem. Soc*. **1996**, *143*, 1114.
(6) Ménétrier, M.; Saadoune, I.; Levasseur, S.; Delmas, C. *J. Mater. Chem.* **1999**, *9*, 1135.
(7) Levasseur, S.; Ménétrier, M.; Suard, E.; Delmas, C. *Solid State Ionics* **2000**, *128*, 11.
(8) Karelina, V. V.; Kellerman, D. E.; Gorshkov, V. S.; Leonidov, I. A.; Patrakeev, M. V. *Russ. J. Phys. Chem*. **2001**, *75*, 496.
(9) Uchimoto, Y.; Sawada, H.; Yoo, T. *J. Synchrotron. Rad.* **2001**, *8*, 872.
(10) Montoro, L. A.; Abbate, M.; Rosolen, J. M. *Electrochem. Solid-State Lett*. **2000**, *3*, 410.
(11) Rosolen, J. M.; Abbate, M. *Solid. State Ionics* **2001**, *139*, 83.
(12) Aydinol, M. K.; Kohan, A. F.; Ceder, G.; Cho, K.; Joannopoulosw, J. *Phys. Rev. B* **1997**, *56*, 1354.
(13) Van der Ven, A.; Aydinil, M. K.; Ceder, G.; Kresse, K.; Hafner, J. *Phys. Rev. B* **1998**, *58*, 2975.
(14) Koyama, Y.; Tanaka, I.; Kim, Y. S.; Nishitani, S. R.; Hadachi, H. *Jpn. J. Appl. Phys.* **1999**, *38*, 4804.
(15) Molenda, J.; Stoklosa, A.; Bak, T. *Solid State Ionics*. **1989**, *36*, 53.
(16) Molenda, J. *Phys. Status Solidi B* **1989**, *165*, 419.
(17) Molenda, J.; Wilk, P.; Marzec, J. *Solid State Ionics* **1999**, *119*, 19.
(18) Shibuya, M.; Nishina, T.; Matsue, T.; Ukida, I. *J. Electrochem. Soc.* **1996**, *143*, 3157.
(19) Nishizawa, M.; Yamamura, S.; Itoh, T.; Ukida, I. *Chem. Commun.* **1998**, 1631.

(20) Levi, M. D.; Salitra, G.; Markovsky, B.; Teller, H.; Aurbach, D.; Heider, U.; L. Heider *J. Electrochem. Soc*. **1999**, *146*, 1279.

(21) Levi, M. D.; Gamolsky, K.; Aurbach, D.; Heider, U.; Oesten, R. *J. Electroanal. Chem*. **1999**, *477*, 32.

(22) Aurbach, D.; Levi, M. D.; Levi, E.; Teller, H.; Markovsky, B.; Salitra, G.; Heider, U.; Heider, L. *J. Electrochem. Soc*. **1998**, *145*, 3024.

(23) Levi, M. D.; Gamolsky, K.; Aurbach, D.; Heider, U.; Oesten, R.; *Electrochim. Acta* **2000**, *45*, 1781.

(24) Levi, M. D.; Aurbach, D. *J. Phys. Chem. B* **1997**, *101*, 4630.

(25) Sato, H.; Takahaschi, D.; Nishima, T.; Uchida, I. *J. Power Sources* **1997**, *68*, 540.

(26) Dokko, K.; Mohamedi, M.; Fujita, Y.; Itoh, T.-; Nishizawa, M.; Umeda, M.; Uchida, I. *J. Electrochem. Soc.* **2001**, *148*, A422.

(27) Croce, F.; Nobili, F.; Deptula, A.; Lada, W.; Tossici, R.; D'Epifanio, A.; Scrosati, B.; Marassi, R. *Electrochem. Comm.* **1999**, *1*, 605.

(28) Nobili, F.; Tossici, R.; Croce, F.; Scrosati, B.; Marassi, R. *J. Power Sources* **2000**, *98*, 238.

(29) Nobili, F.; Croce, F.; Scrosati, B.; Marassi, R. *Chem. Mater*. **2001**, *13*, 1642.

(30) Boukamp, B. A. *Solid State Ionics* **1986**, *20*, 159.

(31) Bruce, P. G.; Saidi, M. Y. *J. Electroanal. Chem.* **1992**, *322*, 93.

(32) Randles, J. E. B. *Trans. Faraday Soc*. **1955**, *56*, 54.

(33) Granqvist, C. G. *Appl. Phys. A* **1993**, *57*, 32.

(34) Raistrick, J. D. *Solid State Ionics*. **1983**, *9*, 425.

(35) Macdonald, J. R. In *Impedance Spectroscopy. Emphasizing Solid Materials and Systems*; Wiley: New York, 1987; p 252.

(36) Varsano, F.; Decker, F.; Masetti, E.; Croce, F. *Electrochim. Acta*. **2001**, *46*, 2069.